useful for our purposes. In any event, it is our hope that accurate experimental data at high energies ($p_L \gtrsim 5$ GeV/c) will soon be available on all these double-charge-exchange reactions.

Lastly, in our calculations, strict $SU(3)$ invariance, with the exception of physical masses for mesons and baryons, has been assumed. However, if necessary, $SU(3)$ symmetry-breaking effects can be easily introduced into the calculations by (e.g.) treating the strange quark differently from the nonstrange quarks. At the present time, we do not see any necessity of introducing $SU(3)$ symmetry-breaking effects into the calculations.

PHYSICAL REVIEW D VOLUME 3, NUMBER 5 1 MARCH 1971

Asymptotic Single-Particle Distributions in the Multiperipheral Model*

N. F. Bali, A. Pignotti, and David Steele
Department of Physics, University of Washington, Seattle, Washington 98105
(Received 17 August 1970)

The conjectures of Feynman and of Benecke, Chou, Yang, and Yen on the high-energy limit of single-particle distributions are studied in the framework of the multiperipheral model. It is found that classes of multiperipheral diagrams add to give limiting single-particle distributions.

I. INTRODUCTION

THE great complexity of inelastic hadronic interactions at high energies has led both theorists and experimentalists to focus their attention on inclusive experiments.[1] They offer the advantages of being easy to perform and relatively simple to describe from a theoretical point of view. This simplicity is a consequence of the summation over all the unobserved channels, which tends to average out the details of the matrix element and to exhibit only its dominant features.

The examples of inclusive experiments that we discuss here are single-particle distributions. Feynman[1] has recently proposed to describe these distributions in the center-of-mass system by means of the double differential cross section $d^2\sigma/dxdq_\perp$, where $x=2q_{\parallel}(s)^{-1/2}$; here $s^{1/2}$ is the total energy, and $q_\perp$ and $q_{\parallel}$ are the transverse and longitudinal components of the momentum of the observed particle. The cross section is then written in the form

$$\frac{d^2\sigma}{dxdq_\perp} = \frac{q_\perp}{\bar{x}} f(x,q_\perp,s), \tag{1.1}$$

where

$$\bar{x}=[x^2+(q_\perp{}^2+\mu^2)/\tfrac{1}{4}s]^{1/2} \tag{1.2}$$

and μ is the mass of the observed particle. Feynman's conjecture is that at very high s the function f becomes energy independent, i.e.,

$$\frac{d^2\sigma}{dxdq_\perp} \xrightarrow[s\to\infty]{} \frac{q_\perp}{\bar{x}} f(x,q_\perp). \tag{1.3}$$

A similar hypothesis was independently formulated by Benecke *et al.*,[2] who describe the same process at finite momenta in the laboratory and projectile frames, and conjecture that $d^2\sigma/dq_{\parallel}dq_\perp$ approaches a constant limit in those frames as $s\to\infty$. In this limit, any finite momentum in the laboratory or projectile frame transforms into a nonzero value of x in the range $-1<x<1$. Conversely, any finite momentum in the center-of-mass system, or in any "intermediate" frame reached from the c.m. frame by a boost of order s^η, $0<\eta<\frac{1}{2}$, goes to the point $x=0$. The conjecture of Benecke *et al.* turns out to be equivalent to Feynman's hypothesis for $x\neq 0$. The point $x=0$, which concentrates all the information of finite momenta in this continuum of frames, is, however, very important, and for this reason we adopt Feynman's notation in our present work.

Our main purpose is to study the high-energy limit of single-particle distributions in the multiperipheral model that was used by Caneschi and Pignotti[3] to fit experimental single-particle distributions at accelerator energies. We point out that in the description of an inclusive experiment we cannot restrict the model to the multi-Regge region of low multiplicities and large subenergies, which only accounts for a small part of the inelastic cross section, but we have to use the model for all multiplicities and throughout phase space, and we can only expect it to be meaningful in some average sense.[4] If we increase the total energy, this approximation is not improved as the additional energy

* Work supported in part by the Atomic Energy Commission and the National Science Foundation.

[1] R. P. Feynman, Phys. Rev. Letters **23**, 1415 (1969).

[2] J. Benecke, T. T. Chou, C. N. Yang, and E. Yen, Phys. Rev. **188**, 2159 (1969).

[3] L. Caneschi and A. Pignotti, Phys. Rev. Letters **22**, 1219 (1969).

[4] G. F. Chew and A. Pignotti, Phys. Rev. Letters **20**, 1078 (1968).

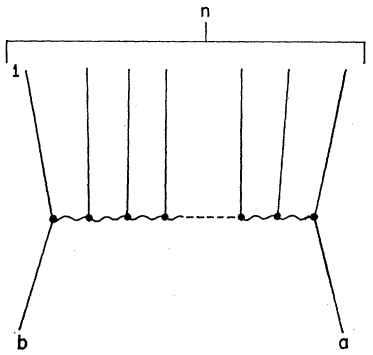

FIG. 1. Typical multiperipheral process: $2 \to n$.

is used in the production of new particles and the average subenergy of a pair of particles emitted at neighboring vertices stays constant. As a consequence, the highest trajectories do not necessarily dominate, and, in particular, we can, as a first approximation, neglect Pomeranchukon exchange in the spirit of Ref. 5.

In this paper we show that Feynman's conjecture is realized by this model and discuss what classes of multiperipheral diagrams contribute at $x \neq 0$ and at $x=0$. We also derive a very simple expression for $f(x,q_\perp)$ for the pion spectrum at small x, which has a number of attractive features.

In Sec. II we discuss multiperipheral diagrams in which the observed particle is emitted at either end of the multiperipheral chain. Section III is devoted to the case of particles emitted at internal vertices of the chain. We discuss the pion and nucleon single-particle distributions in pp collisions and point out some differences between the two. In Sec. IV we summarize our results and discuss them in the context of Refs. 1 and 2. The Appendix contains some details of the integrations performed in the $s \to \infty$ limit.

II. TWO-VERTEX DIAGRAMS

Let us consider particle production in collisions of two particles of equal mass m. The cross section for n particles in the final state can be written as

$$d\sigma^n = |M_n|^2 \lambda^{-1/2}(s,m^2,m^2) d\Phi^n , \qquad (2.1)$$

where $d\Phi^n$ is the n-body phase space, M_n is the matrix element, and λ the kinematic triangle function. We choose the matrix element to be of the multiperipheral form, diagrammatically indicated in Fig. 1, and we start by considering the distribution of particles emitted at either end. For concreteness, we choose particle b to be incident along the positive z direction, and particle 1 to be the observed one. Characteristic of multiperipheral models is factorization of the matrix element into vertex functions that are strongly damped for large values of the invariant momentum transfers and propagators associated with the exchanged objects. In particular we shall consider Regge exchanges characterized by a trajectory function $\alpha_E(t)$, but most of our conclusions are independent of the detailed nature of the exchange. Equation (3) can then be rewritten

$$d\sigma^n = |M_{n-1}|^2 R(s,s',t)\beta(t) \times \lambda^{-1/2}(s,m^2,m^2) d\Phi^{n-1} d\Phi^2 ds' . \qquad (2.2)$$

Here R is the Regge propagator, β contains the factorized dependence of the residue functions on the invariant momentum transfer t,[6] and the n-particle phase space is written as the product of a two-body phase space, times the phase space for the decay of one of these two bodies, of mass $(s')^{1/2}$, into the remaining $n-1$ final particles. The techniques of the integral equation of Chew, Goldberger, and Low[7] and Halliday and Saunders[8] can now be used to perform the integration over $d\Phi^{n-1}$ and the sum over n, and lead to power behavior in s'. We denote this power by $\alpha(0)$, and obtain

$$d\sigma \sim \left(\frac{s'}{m^2}\right)^{\alpha(0)} R(s,s',t)\beta(t)\lambda^{-1/2}(s,m^2,m^2) \frac{q_\perp dq_\perp dx}{\bar{x}} . \qquad (2.3)$$

Note that $\alpha(0)$ is the power generated by an infinite sum of multiperipheral diagrams depicted in Fig. 2, and is in general different from the value of the intercept of the exchanged trajectory considered, $\alpha_E(0)$. Equation (2.3) can be interpreted as incorporating into the model the statement of power behavior for the cross section for inelastic collisions between the exchanged Reggeon and the target particle a.

Asymptotically, the Regge propagator depends on the quotient s/s' in the form

$$R(s/s',t) \sim (s/s')^{2\alpha_E(t)} . \qquad (2.4)$$

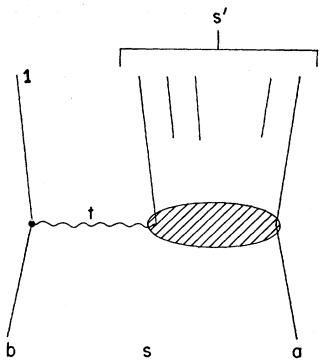

FIG. 2. Typical two-vertex diagram.

[5] G. F. Chew and A. Pignotti, Phys. Rev. **176**, 2112 (1968).

[6] We neglect the Toller-angle dependence of the internal multi-Regge-pole vertex, and assume that the dependence on the adjacent momentum transfers factorizes. We believe that the conclusions of this paper are independent of these approximations.

[7] G. F. Chew, F. E. Low, and M. L. Goldberger, Phys. Rev. Letters **23**, 258 (1969).

[8] I. G. Halliday and L. M. Saunders, Nuovo Cimento **60A**, 115 (1969).

Therefore, we obtain

$$\frac{d^2\sigma}{dq_\perp dx} \underset{s\to\infty}{\sim} \frac{q_\perp}{\bar{x}}\left(\frac{s}{s'}\right)^{2\alpha_E(t)-1}\beta(t)\left(\frac{s'}{m^2}\right)^{\alpha(0)-1}. \quad (2.5)$$

In the limit of $s\to\infty$ and fixed x and $q_\perp$, we have

$$\bar{x}=\begin{cases} x+O(1/s) & \text{for } x>0 \\ O(s^{-1/2}) & \text{for } x=0 \\ -x+O(1/s) & \text{for } x<0, \end{cases} \quad (2.6)$$

and hence, if we call q the four-vector of the observed particle, we have

$$t=(q-p_b)^2=\mu^2+m^2(1-\bar{x})-2\frac{q_\perp^2+\mu^2}{x+\bar{x}}+O(1/s)$$

$$\sim\begin{cases} \text{const for } x>0 \\ s^{1/2} \text{ for } x=0 \\ s \text{ for } x<0 \end{cases} \quad (2.7a)$$

and

$$s/s'=1/(1-\bar{x})+O(1/s). \quad (2.7b)$$

It follows from Eqs. (2.5) and (2.7) that the contribution of the diagram of Fig. 2 is of the Feynman form for $x>0$, provided that $\alpha(0)=1$. This last condition corresponds to a constant Reggeon-particle total cross section. For $x\leq 0$, $|t|$ grows without bound as $s\to\infty$ and therefore both f and $d^2\sigma/dxdq_\perp$ vanish as a consequence of the assumed rapid decrease of β with negative values of t. Of course, in the case of identical incident particles, f is an even function of x, and this symmetry is guaranteed by adding the contributions of the corresponding series of diagrams in which the particle emitted at the right-hand vertex of Fig. 1 is observed.

Let us consider as an example pp collisions in which all inelastic processes except pion production are neglected. The diagram of Fig. 2 contributes to the pion or proton spectrum, depending on the baryon number of the Regge exchange. These two cases are, however, qualitatively different, because of the small ratio between the pion and nucleon mass, as pointed out in Ref. 3. Whereas for a final proton the largest (i.e., less negative) value of t at fixed $q_\perp$ occurs at $x=1$ and therefore we expect the cross section to peak towards this value, for a pion it occurs at $x=[(q_\perp^2+\mu^2)/m^2]^{1/2}$, which is in average approximately equal to 0.4. As a consequence, pions tend to be produced less forward than heavier particles, such as, for instance, kaons. This prediction is qualitatively consistent with cosmic-ray observations,[9] and may even provide an explanation of the Aleph phenomenon.[10]

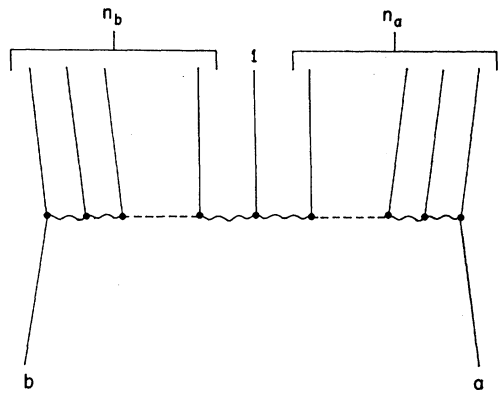

FIG. 3. Typical multiperipheral process in which a particle emitted at an internal vertex is observed, with $n=n_a+n_b+1$.

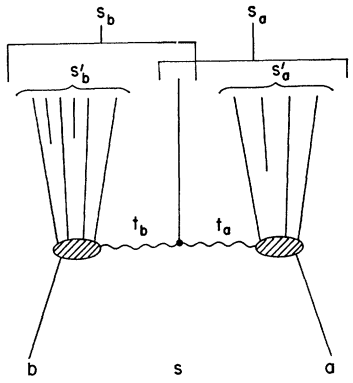

FIG. 4. Typical three-vertex diagram.

III. THREE-VERTEX DIAGRAMS

A. Pion Spectrum

We now consider the distributions of particles emitted at internal vertices in the multiperipheral chain, as depicted in Fig. 3. The n-body phase space is written this time as a three-particle phase space times the phase space for the decay of two of these particles, of masses squared s_a and s_b, into n_a and n_b particles, with $n=n_a+n_b+1$. The total spectrum follows after summation over n and n_a or, equivalently, n_a and n_b, which leads, after using the CLGHS[7,8] results twice, to the form

$$\frac{d^2\sigma}{dq_\perp dx}=\frac{q_\perp}{\bar{x}}\lambda^{-1/2}(s,m^2,m^2)\int\left(\frac{s_{a'}}{m^2}\right)^{\alpha_a(0)}\left(\frac{s_{b'}}{m^2}\right)^{\alpha_b(0)}$$
$$\times R_a\left(\frac{s_a}{s_{a'}},t_a\right)R_b\left(\frac{s_b}{s_{b'}},t_b\right)\beta_a(t_a)\beta_b(t_b)$$
$$\times\frac{\lambda^{1/2}(s',s_a',s_b')}{s'}d\Omega ds_a'ds_b', \quad (3.1)$$

which is represented by the three-vertex diagram of Fig. 4. Just as before, s' is the missing mass squared, which is now shared by the two "blobs" of Fig. 4, and $[\lambda^{1/2}(s',s_a',s_b')/s']d\Omega$ is the phase space for the decay

[9] C. O. Kim, Phys. Rev. **136**, B515 (1964).
[10] M. Koshiba, in *Proceedings of the Third International Conference on High-Energy Collisions, Stony Brook, 1969* (Gordon and Breach, New York, 1969), p. 165.

of s' into two blobs of masses s_a' and s_b' in their center-of-mass frame. Equation (3.1) involves a four-dimensional integration, and the study of its high-energy limit is somewhat involved. The analysis is simplified if we choose exponential parametrization of the residue functions

$$\beta_a(t)=\beta_b(t)=e^{\Omega t} \tag{3.2}$$

and, furthermore, neglect the effect of the slope of the Regge trajectories in the propagators

$$R(s/s',t)\approx(s/s')^{2\bar{\alpha}_E}. \tag{3.3}$$

The limited range of values of t which contribute substantially to the cross section makes it reasonable to approximate $\alpha_E(t)$ by some average value $\bar{\alpha}_E$. In the limit of large s, we can evaluate the leading behavior of the integrals in Eq. (3.1). The details are presented in the Appendix; we discuss the results here.

For concreteness, we go back to the example of nucleon-nucleon collisions with production of only pions, and we begin by considering the pion spectrum. The observed pion can be emitted at either a meson or a baryon exchange vertex. In the first case, both blobs of Fig. 4 carry baryon number 1 and represent the total baryon–Reggeized-meson cross section. We assume Pomeranchukon behavior for this, i.e., $\alpha_a(0)=\alpha_b(0)=1$, and we take $\bar{\alpha}_E$ to represent a typical meson trajectory exchanged. We call this case the Pomeranchukon-Pomeranchukon (PP) three-vertex diagram, and obtain [see Eq. (A9)]

$$\frac{d^2\sigma}{dq_\perp dx}=\frac{q_\perp}{\bar{x}}e^{\Omega\tau}I(q_\perp,x), \tag{3.4}$$

where, if we set the threshold mass m_b of blob b equal to the nucleon mass, τ is given by

$$\tau=-\frac{q_\perp^2}{2-x}-\frac{m^2x^2}{1-x} \tag{3.5}$$

and represents the maximum value of t_1+t_2 attainable in the region of integration of Eq. (3.1) for given values of x and $q_\perp$, as $s\to\infty$. The function $I(q_\perp,x)$ involves a one-dimensional integration, depends on Ω and $\bar{\alpha}_E$, has no zeros for $|x|<1$, and contains no further exponential dependence. If we choose to ignore this function, we are left with a simple expression for the pionic asymptotic single-particle distribution which has a number of appealing features. (i) It exhibits Feynman's limit, including the point $x=0$, which gives rise to a logarithmic growth of multiplicity with energy. (ii) It is strongly damped for large values of $q_\perp$, as a consequence of the input damping in t. (iii) It suggests a simple form for function f, which, for small x, approximately factorizes in its dependence on x and $q_\perp$, and has a Gaussian dependence on x. Note that the latter also follows from the original exponential dependence of the residue function on the invariant momentum transfers. All the above features appear to be qualitatively correct.[11]

We now consider the case in which the pion is emitted by a baryon-exchange line, and we set $\bar{\alpha}_E$ equal to some average baryon trajectory $\bar{\alpha}_B$. In this case, one blob, for example the one with index a, carries baryon number 2, and describes the baryon–Reggeized-baryon total cross section, whereas the other blob contains no baryonic lines in the final state and corresponds to the cross section for baryon–Reggeized-antibaryon annihilation into pions. This cross section is not expected to be constant, but rather to decrease with energy like some inverse power. In other words, we set

$$\alpha_a(0)=1,\quad a_b(0)=\alpha_A<1.$$

We call this contribution the three-vertex Pomeranchukon-annihilation (PA) diagram, and we find, for $x>0$, as indicated in the Appendix,

$$\frac{d^2\sigma}{dq_\perp dx}=\frac{q_\perp}{\bar{x}}e^{\Omega\tau}I'(q_\perp,x), \tag{3.6}$$

with

$$\tau=-\frac{x^2m^2}{1-x}-\frac{q_\perp^2}{2-x}-(m^2-m_b^2)\frac{2-3x}{2(1-x)}, \tag{3.7}$$

where m_b is the threshold mass for the b blob. The function I' has properties similar to those of I mentioned above. For $x<0$, the same result with a replaced by b and x by $-x$ holds. Thus we see that those diagrams in which the pion is emitted at a baryon-exchange line again have a nonvanishing limit for f but only for positive values of x with the above choice for $\alpha_a(0)$ and $\alpha_b(0)$. At $x=0$, from Eq. (A11)

$$\left.\frac{d^2\sigma}{dxdq_\perp}\right|_{x=0}=\frac{q_\perp}{\bar{x}}e^{\Omega\tau}I_0(q_\perp)\left(\frac{s}{m^2}\right)^{\frac{1}{2}[\alpha_a(0)+\alpha_b(0)]-1}, \tag{3.8}$$

with $\tau=-q_\perp^2/2$. Hence,

$$f(0,q_\perp,s)\sim s^{\frac{1}{2}(\alpha_A-1)} \tag{3.9}$$

as $s\to\infty$. In other words, Pomeranchukon behavior is required for both blobs if we want to find a nonvanishing value of $f(0,q_\perp)$. In the language of Ref. 2, pions emitted at a baryon line correspond to "fragments" of that baryon, and give rise to finite asymptotic cross sections $d^2\sigma/dq_\parallel dq_\perp$ in the frame in which the corresponding incident baryon is at rest. The same is true for the two-vertex diagrams described in Sec. II.

B. Nucleon Spectrum

The same analysis can be applied to the nucleon spectrum. Because we have ignored nucleon-antinucleon pair production, we expect a finite multiplicity and therefore a vanishing $f(0,q_\perp)$. If we want to be more precise, we can say that our model applies to the difference between the final nucleon and antinucleon spectra, and in this way subtract out the effect of

[11] N. Bali, L. S. Brown, R. Peccei, and A. Pignotti, Phys. Rev. Letters 25, 557 (1970).

nucleon-antinucleon pair production ("nucleonization"). The latter is expected to be present, and the model can be extended to account for it. A three-vertex PP diagram analogous to the one described for the pion spectrum provides this effect. Its coefficient, however, appears to be small,[12] and that is why we choose to neglect it in our example.

Even in the absence of nucleonization, we observe from formulas (1.1), (2.6), and (3.9) that the proton *cross section* does not vanish asymptotically at $x=0$ if $\alpha_A \geq 0$. If we choose α_A to be the ω Regge-trajectory intercept, i.e., $\alpha_A \approx 0.5$,[13] we find

$$\left.\frac{d^2\sigma}{dx dq_\perp}\right|_{x=0} \propto s^{1/4}.$$

Thus the contribution of the three-vertex diagram to the proton spectrum at $x=0$ would show a weak rise with energy, in contrast to the decrease of the two-vertex diagrams discussed above. Phenomenologically, neither an increase nor a decrease is yet observed in experiments at accelerator energies, and the behavior of the proton spectrum, after subtraction of the nucleonization effect, remains an interesting problem.

IV. CONCLUSIONS

We have found that the multiperipheral model satisfies Feynman's scaling limit given the assumption of constant Reggeon-particle total cross sections.[14] We have discussed two types of diagrams: those in which only one blob with Pomeranchukon behavior is present, and the one in which the observed particles lies between two blobs with Pomeranchukon behavior. The former describe effects associated with one end of the multiperipheral chain, and are characterized by the presence of the Pomeranchukon blob at the *other* end. The observed particle is either emitted at an external vertex, such as in the two-vertex diagram, or separated from it by a non-Pomeranchukon blob, as in the three-vertex PA diagram. In either case, f vanishes at $x=0$ and at either positive or negative values of x, depending on whether the observed particle is associated with the projectile (b) or target (a) end of the chain. In the language of Ref. 2, these diagrams may be interpreted as describing fragments of the projectile or of the target. The average multiplicity for these diagrams is, however, constant. The second type of diagram scales for $-1<x<1$, and the corresponding multiplicity is logarithmically divergent with s, because the function f is regular and nonvanishing at $x=0$. The distributions $d^2\sigma/dq_{\parallel}dq_\perp$ from this diagram are asymptotically different from zero in the laboratory, projectile, and all other intermediate frames, including the c.m. Therefore, this diagram satisfies the properties of limiting fragmentation of Benecke *et al.*,[2] and of pionization of Cheng and Wu.[15] Note, however, that it gives rise to a smooth distribution $f(x)$, with no breaks that would allow us to split its contribution into fragments of the target, of the projectile, and pionization products.

APPENDIX

We discuss here the evaluation of the integrals of Eq. (3.1) as $s\to\infty$, with the approximations of Eqs. (3.2) and (3.3), for $x>0$ and $x=0$. Our task is simplified if we evaluate the integrals in the c.m. frame for the decay of a missing mass $(s')^{1/2}$ into two masses $(s_a')^{1/2}$ and $(s_b')^{1/2}$, and in which the relative incident momentum $\mathbf{P}_b-\mathbf{P}_a$ points along the z direction. In this frame, the orientation of the momentum of the b blob is specified by two angles θ and ϕ, upon which we integrate. We have

$$f(x,q_\perp)\sim s^{-1}\int (s_a')^{\alpha_a(0)}(s_b')^{\alpha_b(0)}\left(\frac{s_a}{s_a'}\right)^{2\alpha_{Ea}}\left(\frac{s_b}{s_b'}\right)^{2\alpha_{Eb}} \times\exp[\Omega(t_a+t_b)]\frac{\lambda^{1/2}(s',s_a',s_b')}{s'}d\Omega ds_a' ds_b', \quad \text{(A1)}$$

with

$$t_a+t_b=u\cos\theta+v,$$

$$u=s\lambda^{1/2}\left(1,\frac{s_a'}{s'},\frac{s_b'}{s'}\right)\lambda^{1/2}\left(1,\frac{m^2}{s},\frac{m^2}{s}\right) \times\left(\frac{s'}{s'+q_\perp^2}\right)^{1/2}\left[\left(1-\frac{\bar{x}}{2}\right)^2+\frac{x^2q_\perp^2}{4s'}\right]^{1/2}, \quad \text{(A2)}$$

$$v=2m^2+s_a'+s_b'-s\left(1-\frac{\bar{x}}{2}\right) -\frac{s_a'-s_b'}{s'}\frac{sx}{2}\lambda^{1/2}\left(1,\frac{m^2}{s},\frac{m^2}{s}\right). \quad \text{(A2)}$$

When $s\to\infty$, u grows linearly with s, and the integral over $\cos\theta$ can be estimated using asymptotic techniques:

$$f(x,q_\perp)=\int e^{\Omega v}\int_{-1}^{1} e^{\Omega u\cos\theta}F(\theta) \times d\cos\theta d\phi\approx F(0)\frac{e^{(u+v)\Omega}}{u}. \quad \text{(A3)}$$

[12] See, for instance, the data at 19.2 GeV of J. W. Allaby *et al.*, in *Proceedings of the Fourteenth International Conference on High-Energy Physics, Vienna, 1968*, edited by J. Prentki and J. Steinberger (CERN, Geneva, 1968).

[13] P. Ting, Phys. Rev. **181**, 1942 (1969).

[14] Amati, Stanghellini, and Fubini have also discussed single-particle distributions in the multiperipheral model [see D. Amati, A. Stanghellini, and S. Fubini, Nuovo Cimento **26**, 896 (1962), and also the article by S. Fubini, in *Strong Interactions and High-Energy Physics*, edited by R. G. Moorhouse (Plenum, New York, 1964), p. 259]. In the case of the three-vertex diagram, however, these authors effectively limit their discussion to the point $x=0$, and, therefore, do not arrive at Feynman's scaling law.

[15] H. Cheng and T. T. Wu, Phys. Rev. Letters **23**, 1311 (1969). Note, however, that a different definition of pionization is adopted by T. T. Chou and C. N. Yang, Phys. Rev. Letters **25**, 1072 (1970). If we use the latter definition, the multiperipheral model predicts that the pionization disappears like $(\ln s)^{-1}$ at high energies.

Neither u, v, nor $F(0)$ depend on the azimuthal angle ϕ, and thus this integral is trivial.

From Eqs. (A2) and (A3) the argument of the exponential is a monotonic function of s_b' which decreases with increasing s_b'. In the approximation of large Ω, which turns out to be good for typical experimental values of this damping coefficient, we can keep only the constant and linear terms in the expansion of the exponent as a function of s_b', and write for the resulting integral

$$\int_{m_b^2} ds_b' e^{-\chi s_b'} G(s_b',\delta)(s_b')^{\alpha_b(0)} \approx G(m_b^2,\delta)\int_{m_b^2} ds_b' e^{-\chi s_b'}(s_b')^{\alpha_b(0)} \approx G(m_b^2,\delta)\Gamma[\alpha_b(0)+1,\chi m_b^2]\chi^{-\alpha_b(0)-1}, \quad \text{(A4)}$$

where

$$G(s_b',\delta)=\left\{1+\frac{x}{(1-x)(1-\delta)}+\frac{\mu^2}{s_b'}\left[1+\frac{(1-\delta)(1-x)}{x}\right]+\frac{4q_\perp^2}{s_b'}\frac{(1-x)(1-\delta)}{x(2-x)^2}\right\}^{2\alpha_{Eb}}, \quad \text{(A5)}$$

$$\chi=\Omega\left(\frac{2-x}{1-x}\frac{1}{1-\delta}-2\right), \quad \text{(A6)}$$

and

$$\delta=s_a'/s'.$$

The upper limit in this integral grows with s and its contribution can be neglected.

The remaining integral can be performed numerically. We describe the case in which $\alpha_b(0)=1$, but different values of $\alpha_b(0)$ can be treated in the same fashion, and lead to the same type of results for $x>0$. We have

$$f\sim\frac{(1-x)^2}{2-x}(s')^{\alpha_a(0)-1}\exp\left\{\Omega\left[m^2(x+2)-\frac{q_\perp^2}{2-x}+\frac{(m_b^2-m^2)(2-3x)}{2(1-x)}\right]\right\}\int_0^1 d\delta\,\delta^{\alpha_a(0)}G(m_b^2,\delta)\times\left[1+\frac{x}{\delta(1-x)}\right]^{2\bar{\alpha}_{Ea}}\frac{e^{A\delta-B/(1-\delta)}}{\chi}\left(\frac{1}{\chi}+m^2\right), \quad \text{(A7)}$$

with

$$A=\Omega\left[2m^2(1-x)-\frac{2q_\perp^2(1-x)}{x(2-x)}+\mu^2\left(1-\frac{1}{x}\right)\right]$$

and

$$B=\Omega\frac{2-x}{1-x}m^2. \quad \text{(A8)}$$

Note that here the value of $\alpha_a(0)$ plays an essential role, in contrast with $\alpha_b(0)$. The cross section is nonvanishing in the $s\to\infty$ limit only for $\alpha_a(0)=1$. The change of variables

$$y^2=-A\delta+B/(1-\delta)-B$$

leads to the following expression for $f(x,q_\perp)$, valid when $x>0$:

$$f(x,q_\perp)\sim e^{\Omega\tau}(s')^{\alpha_a(0)-1}\int_0^\infty e^{-y^2}H(y,x,q_\perp)dy, \quad \text{(A9)}$$

where

$$\tau=\frac{-x^2m^2}{1-x}-\frac{q_\perp^2}{2-x}-\frac{m^2-m_b^2}{2(1-x)}(2-3x)$$

and the function H does not contain exponentials.

If we now consider the point $x=0$, we can proceed as before up to Eq. (A3). It is now important to notice that $\bar{x}\propto s^{-1/2}$, and as a consequence, the coefficient of s_b' in the exponential is also of order $s^{-1/2}$, namely,

$$\chi=2\Omega(q_\perp^2+\mu^2)/\sqrt{s}. \quad \text{(A10)}$$

The integral over s_b' is again of the form (A7) and yields a factor $s^{[\alpha_b(0)+1]/2}$. By symmetry an analogous factor comes from the s_a' integral, so that we obtain

$$f(0,q_\perp)\sim e^{\Omega\tau_0}(s/m^2)^{[\alpha_a(0)+\alpha_b(0)]/2-1}I_0(q_\perp), \quad \text{(A11)}$$

where now

$$\tau_0=-\tfrac{1}{2}q_\perp^2.$$

A factor s^{-2} has been picked up from the s^{-1} in Eq. (A1) and $1/u$ in Eq. (A3).

Finally, we would like to remark that we have performed numerical comparisons between our asymptotic formulas and calculations with the nonasymptotic expressions at 30 GeV/c for reasonable values of the parameters, and found the agreement to be within 15%